

Mutually attracting spin waves in the square-lattice quantum antiferromagnet

M. Powalski,^{1,*} K. P. Schmidt,^{2,†} and G. S. Uhrig^{1,‡}

¹*Lehrstuhl für Theoretische Physik I, Technische Universität Dortmund,
Otto-Hahn Straße 4, 44221 Dortmund, Germany*

²*Lehrstuhl für Theoretische Physik I, Staudtstraße 7,
Universität Erlangen-Nürnberg, D-91058 Erlangen, Germany*

(Dated: January 18, 2017)

The Heisenberg model for $S = 1/2$ describes the interacting spins of electrons localized on lattice sites due to strong repulsion [1]. It is the simplest strong-coupling model in condensed matter physics with wide-spread applications. Its relevance has been boosted further by the discovery of cuprate high-temperature (T_c) superconductors [2]. In leading order, their undoped parent compounds realize the Heisenberg model on square-lattices [3]. Much is known about the model [4–7], but mostly at small wave vectors, i.e., for long-range processes, where the physics is governed by spin waves (magnons), the Goldstone bosons of the long-range ordered antiferromagnetic phase. Much less, however, is known for short-range processes, i.e., at large wave vectors. Yet these processes are decisive for understanding high T_c superconductivity [8–11]. Recent reports

suggest that one has to resort to qualitatively different fractional excitations, spinons [12–15]. By contrast, we present a comprehensive picture in terms of dressed magnons with strong mutual attraction on short length scales, see Fig. 1. The resulting spectral signatures agree strikingly with experimental data.

Understanding the magnetic glue in high T_c superconductors is still one of the holy grails in condensed matter physics. Yet evidence is growing that magnetic fluctuations take over the role played by phonons in conventional superconductors [10, 11, 16]. But it is the magnetic fluctuations at large wave vectors, i.e., at high energies, which matter [8–11]. This clearly shows the importance of short-range processes. One has to be able to describe the hole-magnon interaction quantitatively. Even this turns out to be an intricate issue still subject to debate [16].

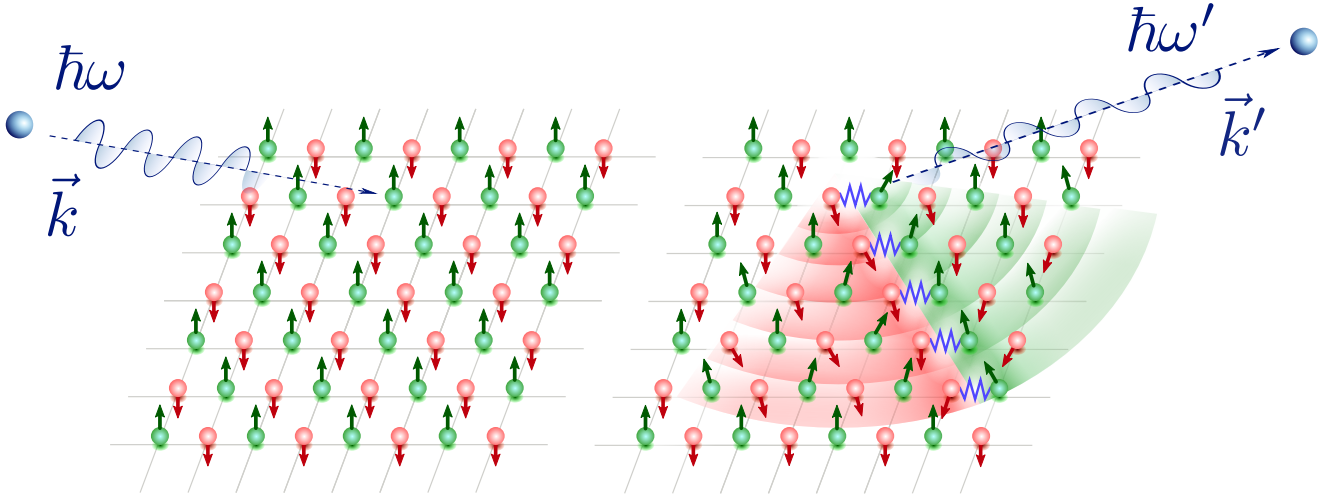


FIG. 1. **Sketch of a scattering event** By inelastic scattering of a neutron two magnons are excited from the long-range ordered antiferromagnetic ground state. On short distances, they interact strongly and attract each other forming resonances [17].

Even more surprisingly, the problem without charge degrees of freedom, that is the undoped Heisenberg model

with nearest-neighbor antiferromagnetic exchange interaction between spins with $S = 1/2$

$$H = J \sum_{\langle i,j \rangle} \vec{S}_i \cdot \vec{S}_j \quad (1)$$

* michael.powalski@tu-dortmund.de

† kai.phillip.schmidt@fau.de

‡ goetz.uhrig@tu-dortmund.de

poses issues for large wave vectors. Previously, series expansions about the Ising limit and a quantum Monte

Carlo approach were able to compute the roton minimum [18] at $\mathbf{k} = (\pi, \mathbf{0})$ while a direct expansion in the inverse spin length turned out to be insufficient even in third order [19]. The seeming failure of the magnon description is due to an insufficient understanding of short-range processes, constituting a long-standing problem. Only recently, we achieved the quantitative description of the roton minimum in the dispersion of the two-dimensional (2D) Heisenberg model on a square-lattice based on an effective model expressed in magnons [17], see also Fig. 2. Nevertheless, it remained an open problem to gain a full theoretical understanding of the spectral signatures and the dynamic correlations of magnetic excitations in the square-lattice quantum antiferromagnet as observed experimentally in inelastic neutron scattering. In this work we solve this challenging quest in terms of dressed magnon excitations. The attractive interactions between these magnons turn out to be crucial in the square-lattice quantum antiferromagnet.

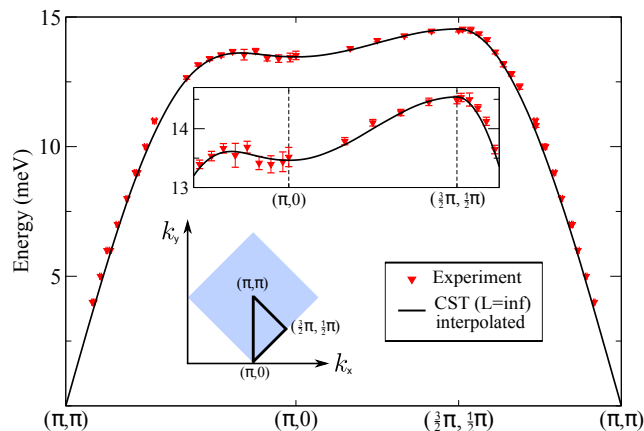


FIG. 2. **One-magnon dispersion.** Representative cut through the magnetic Brillouin zone comparing the dispersion obtained by CST and extrapolated to infinite system size for a mesh of momenta and interpolated between them, see Methods, (solid line) with the experimental data from Ref. 15. The inset shows the agreement around the roton minimum at $(\pi, 0)$.

The key step in our approach in terms of magnons was to take the full renormalization of the magnon dispersion and of their interactions into account. Physically, the attractive magnon-magnon interaction gives rise to the formation of a two-magnon “Higgs” resonance corresponding to a longitudinal magnon with finite lifetime. This resonance in turn is responsible for the formation of the roton minimum due to quantum level repulsion of the associated magnon-Higgs continuum and the single magnon mode [17]. Therefore, it is essential to capture magnon-magnon interactions quantitatively which we achieved technically by a continuous similarity transformation (CST). A running parameter ℓ is used similarly to an inverse energy cutoff. It parametrizes the renormal-

ization flow of the Hamiltonian $H(\ell)$ and is taken from zero to infinity. This is achieved by integrating the flow equation

$$\partial_\ell H(\ell) = [\eta(\ell), H(\ell)]. \quad (2)$$

The antihermitian generator $\eta(\ell)$ determines the form of the flow. We choose the particle conserving generator which comprises the same terms as the Hamiltonian if the terms change the number of magnons. If the balance in the number of magnons is positive the same sign in η is used as in H . If it is negative, the opposite sign is used [17, 20, 21]. At $\ell = \infty$ the effective model is reached which shows the advantageous property to conserve the number of excitations because all net particle creating or annihilating terms are rotated away [20, 22]. Thus this effective model can be analyzed straightforwardly by standard techniques such as the Lanczos approach to resolvents. A subtlety consists in the fact that $H(\ell = \infty)$ is not manifestly hermitian [21].

In order to verify that the reached theoretical description captures the dynamics of real systems it is necessary to compare to measured data. We use the data obtained by inelastic neutron scattering from the compound $\text{Cu}(\text{DCOO})_2 \cdot 4\text{D}_2\text{O}$ [14, 15, 23]. This substance has a an exchange coupling J of about 6meV. This rather low value indicates that the virtual hopping t of electrons between the copper ions is small; recall the leading order relation $J = 4t^2/U$ where U is the local repulsive interaction. A low value of t is advantageous because it implies that higher order corrections are negligible. Hence $\text{Cu}(\text{DCOO})_2 \cdot 4\text{D}_2\text{O}$ is an excellent realization of the antiferromagnetic Heisenberg model with coupling between nearest neighbors.

To understand the data the renormalization of the Hamiltonian by CST or other approaches is not sufficient. The relevant observables O , for instance the spin components S_j^z at lattice site j , need to be included as well. In the framework of the CST this means that they must be transformed as well, according to

$$\partial_\ell O = [\eta(\ell), O(\ell)]. \quad (3)$$

We performed this transformation in parallel to the transformation (2) of the Hamiltonian. Eventually, we are in the position to determine the dynamic structure factor at zero temperature

$$S^{\alpha\alpha}(\omega, \mathbf{Q}) = \frac{-1}{\pi} \text{Im} \langle 0 | S^\alpha(-Q) \frac{1}{\omega - (H_{\text{eff}} - E_0)} S^\alpha(Q) | 0 \rangle \quad (4)$$

with $\alpha = x, y$, or z which is the quantity measured by the counting rate of inelastic neutron scattering. The contributions of different subspaces of the Hilbert space, distinguished by the number of magnons, can be computed separately [17, 21, 22]. This facilitates the computation considerably. If the contribution of more than one single magnon is computed, the interaction of each pair of

them must be taken into account. Previously, this effect was not accounted for in spin wave calculations [24, 25]. The description in terms of an effective $O(3)$ -continuum model with adjusted parameters includes interaction effects, but is tailored to the Raman response, i.e., the response at zero momentum [26]. Hence the results computed for the lattice model by CST promote our understanding of the 2D Heisenberg model to a higher level which was so far beyond reach.

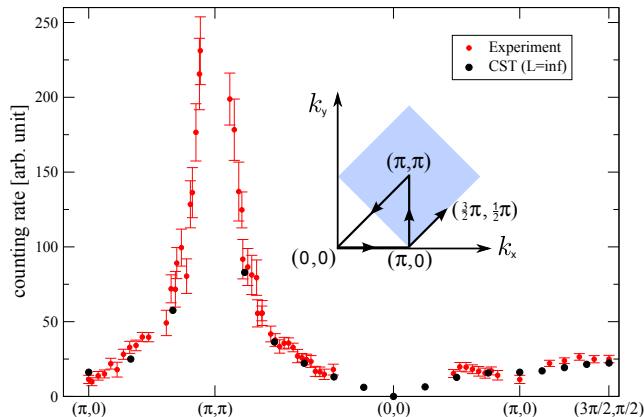


FIG. 3. **Spectral weight of the single magnon excitations.** Comparison of the measured weights from Ref. 14 with the computed weights $S_1^{xx}(Q) + S_1^{yy}(Q)$. An overall factor is fitted.

First, the spectral weight of single magnon excitations is addressed in Fig. 3. The weight constitutes a static quantity providing information about the square modulus of the matrix element with which a magnon is excited. The weights do not provide information about the magnon dynamics. Fig. 3 compares the spectral weight as measured [14] to the theoretical result $S_1^{\alpha\alpha}(Q) := \langle 0 | S^\alpha(-Q) \mathcal{P}_1 S^\alpha(Q) | 0 \rangle$ where $\alpha \in \{x, y, z\}$. The projector \mathcal{P}_1 singles out the subspace of a single magnon which constitutes the dominant contribution. The agreement of measured and computed data is very good and encourages to move on to the dynamics.

The main result is displayed in Fig. 4. The recent experiment allows one to distinguish the longitudinal and the transverse part of the dynamic structure factor. If the antiferromagnetically alternating long-range magnetization is directed in S^z direction, the longitudinal part is $S^{zz}(\omega, Q)$ while the transverse is given by $S^{xx+yy}(\omega, Q) := S^{xx}(\omega, Q) + S^{yy}(\omega, Q)$. Since the magnetic order on the square-lattice is collinear the transverse part is made of the contributions of odd numbers of magnons while the longitudinal part is made of the ones of even numbers. Hence, in the transverse channel, the one-magnon contribution dominates because at fixed total momentum it manifests itself by a resolution limited δ -peak as depicted by the magenta curves in panel (c) and (d) of Fig. 4. Its position allows us to fix the energy scale $J = 6.11(2)$ meV. Besides the one-magnon peaks

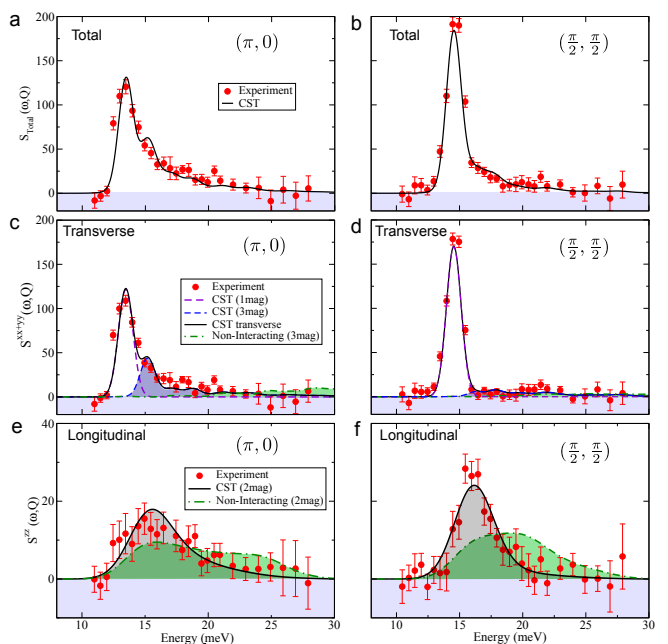


FIG. 4. **Dynamic structure factor.** Comparison between the dynamic structure factors measured in Ref. 15 and the theoretical line shapes obtained from the continuous similarity transformation. For all curves the energy scale is set to $J = 6.11(2)$ meV. Moreover, the units of the y-axis are fixed globally to match the experimental data. The lattice constant is set to unity. (a) Total structure factor (sum of transverse and longitudinal part) at $Q = (\pi, 0)$. (b) Total structure factor at $Q = (\frac{\pi}{2}, \frac{\pi}{2})$. (c) Transverse structure factor at $Q = (\pi, 0)$. The magenta line shows the dominant one-magnon peaks. The broadening is set to $\Delta\omega = 0.58(2)$ meV. The three-magnon continuum is shown as a blue curve; the slightly bumpy behavior stems from discretization effects. Neglecting the interaction leads to the green curve which does not agree with experiment at all. (d) Transverse structure factor at $Q = (\frac{\pi}{2}, \frac{\pi}{2})$; otherwise as (c). (e) Longitudinal structure factor at $Q = (\pi, 0)$. The broadening $\Delta\omega = 1.41(5)$ meV is fixed to match the experimental data. The black line depicts the two-magnon continuum; the four magnon contribution is negligible. The green line results from neglecting the magnon-magnon interaction. (f) Longitudinal structure factor at $Q = (\frac{\pi}{2}, \frac{\pi}{2})$; otherwise as (e).

the three-magnon continuum is important, especially for momentum $Q = (\pi, 0)$. This significant continuum was the key observation in Ref. 15 and led to the claim that a spinon description is indicated.

The broadening and the overall height of the one- and the three-magnon contribution are fitted together to the experimental data. The units of the energy axis and of the y-axis in Fig. 4 are fixed globally for both, the transverse and longitudinal channel together. The agreement achieved is convincing. The crucial importance of the attractive interaction is underlined by the green curve where the interaction between the magnons has been neglected. Then, the magnon result does not match the experimental finding. This conclusion is corroborated by

the very good match in the longitudinal channel including magnon-magnon interaction, see panels (e) and (f) of Fig. 4. Thus, the experimental peak in the longitudinal structure factor can be directly identified with the ‘‘Higgs’’ resonance being a longitudinal magnon with a finite lifetime. The omission of the obviously attractive interaction would lead to a qualitatively wrong result where spectral weight is shifted to the right to larger energies.

In sum, the above results show that the effective magnon model obtained by CST captures the physics of the 2D Heisenberg system quantitatively. Including also the appropriate renormalization of the observables allows us to obtain an impressive agreement with experiment. In particular the continua can be reproduced if the important attractive magnon-magnon interaction is taken into account. This is a crucial aspect because previously the occurrence of the continua was interpreted as evidence for a failure of the magnon description, justifying to search beyond the Goldstone bosons for qualitatively different fractional excitations such as spinons.

In conclusion, the Goldstone bosons of the long-range ordered two-dimensional Heisenberg model not only describe the dynamics at low energies but also at high energies if the magnon-magnon interaction is taken into account quantitatively. Thereby, a crucial step to a truly quantitative understanding of long-range ordered quantum magnetism has been achieved. This also paves the way for determining the magnetic side of high T_c superconductors unambiguously because the values of additional exchange couplings such as the ring exchange [27] can be analyzed. So far, this was hampered by the insufficient accuracy of the theoretical tools.

Methods

We apply the continuous similarity transformation (2). Starting with the initial condition $H(\ell = 0) := H$ (with H given by Eq. (1) expressed in Dyson-Maleev representation) the effective model is obtained by $H_{\text{eff}} := H(\ell = \infty)$. The particle conserving generator $\eta(\ell) = H^+(\ell) - H^-(\ell)$ is used [20] where $H^+(\ell)$ and $H^-(\ell)$ denote the parts of the Hamiltonian which increase (+) or decrease (-) the number of magnons. As a result, the effective model is block-diagonal in the number of magnons [22]. For the dynamic structure factors the representation of the observables in the effective basis is required. Therefore, we apply (3) to the observables $S(Q)^\pm := S(Q)^x \pm iS(Q)^y$ and $S(Q)^z$. The effective observables result from the operators at $\ell = \infty$.

The flowing Hamiltonian and the observables are expressed as normal-ordered bosonic terms with ℓ -dependent coefficients obeying non-linear integro-differential flow equations. To obtain closed equations, they are truncated according to their scaling dimension d [17]. Smaller scaling dimension indicate more relevant terms. The bilinear kinetic energy has $d = 1$; the quartic terms exhibit $d = 2$. Terms with higher scaling

dimension such as hexatic terms are omitted.

In the numerical solution of the flow equations, we use equidistant discretizations of the magnetic Brillouin zone with $N = L \times L$ grid points. The flow equations are integrated with a standard adaptive Runge Kutta Fehlberg 4(5) method for systems with $L = 6$ up to $L = 16$. The coefficients for $L \rightarrow \infty$ are obtained by finite size extrapolation for common grid points. Appropriate interpolation schemes are employed to obtain intermediate points.

At zero temperature, the dynamic structure factor, i.e., the experimental counting rate, is given by the imaginary part of resolvents of the Hamiltonian. Due to the block-diagonality of H_{eff} the required resolvents $R(\omega, Q)$ split into contributions from separate subspaces of different numbers n of magnons

$$R(\omega, Q) = \sum_n \langle 0 | O_{\text{eff}}^{(-n)}(Q) \frac{1}{\omega - (H_{\text{eff}} - E_0)} O_{\text{eff}}^{(+n)}(Q) | 0 \rangle \quad (5)$$

where O^n stands for the part of the effective observable creating n magnons or annihilating $-n$ magnons. As usual, the counting rate is given by the spectral density $I(\omega, Q) = -\frac{1}{\pi} \Im R(\omega, Q)$ where $|0\rangle$ denotes the vacuum state with no magnons, E_0 is the ground state energy.

The transverse dynamic structure factor $S^{xx+yy}(\omega, Q)$ results from $O = S^-(Q)$ and the odd sectors $n = 1$ and $n = 3$ contribute significantly. The longitudinal dynamic structure factor $S^{zz}(\omega, Q)$ results from $O = S^z(Q)$ and the even sectors $n = 2$ dominates. The static dynamic structure factors are given by

$$S_n^\alpha(Q) := \langle 0 | S^\alpha(-Q) \mathcal{P}_n S^\alpha(Q) | 0 \rangle \quad (6)$$

where \mathcal{P}_n projects onto the subspace with n magnons. The longitudinal and transverse static structure factors are obtained in the thermodynamic limit by a finite size extrapolation in $\frac{1}{L}$.

The evaluation of the dynamic structure factors requires to consider the dispersion and the effective two-magnon interaction. To this end, a non-symmetric Lanczos algorithm is applied to determine the continued fraction representation of the resolvent. To decrease finite size effects, we interpolate the coefficients in the Hamiltonian and the observables. For the longitudinal part, the system size is enhanced from $L = 8$ to $L = 192$ in this way. For the transverse part, we use a system size of $L = 16$.

The resulting spectral functions are sums of δ -functions because we truncate the continued fraction where finite size effects set in. The smooth densities are obtained by broadening the truncated continued fractions. We replace the δ -peaks by Gaussian functions with the corresponding weight and the broadenings $\Delta\omega$ given in the caption of Fig. 4. They are determined from fits to the experimental data.

The spectral weights depend slightly on the interpolation of the coefficient resulting from the numerical CST. In particular, the relative weights may be influenced since different interpolation schemes are employed for sectors of different magnon number. To ensure the correct relative weights, we rescale the resulting spectral densities such that they are consistent with the robust static structure factors obtained from reliable finite size extrapolation to the thermodynamic limit.

[1] Harris, A. B. & Lange, R. V. Single-particle excitations in narrow energy bands. *Phys. Rev.* **157**, 295 (1967).

[2] Bednorz, J. G. & Müller, K. A. Possible high- T_c super-

- conductivity. *Z. Phys. B* **64**, 189 (1986).
- [3] Manousakis, E. The spin- $\frac{1}{2}$ Heisenberg antiferromagnet on a square lattice and its application to the cuprous oxides. *Rev. Mod. Phys.* **63**, 1 (1991).
- [4] Reger, J. D. & Young, A. P. Monte Carlo simulations of the spin- $\frac{1}{2}$ Heisenberg antiferromagnet on a square lattice. *Phys. Rev. B* **37**, 5978 (1988).
- [5] Chakravarty, S., Halperin, B. I. & Nelson, D. R. Two-dimensional quantum Heisenberg antiferromagnet at low temperatures. *Phys. Rev. B* **39**, 2344 (1989).
- [6] Auerbach, A. & Larson, B. E. Doped antiferromagnet: The instability of homogeneous magnetic phases. *Phys. Rev. B* **43**, 7800 (1991).
- [7] Sandvik, A. W. Finite-size scaling of the ground-state parameters of the two-dimensional Heisenberg model. *Phys. Rev. B* **56**, 11678 (1997).
- [8] Vignolle, B. et al. Two energy scales in the spin excitations of the high-temperature superconductor $\text{La}_{2-x}\text{Sr}_x\text{CuO}_4$. *Nature Phys.* **3**, 163 (2007).
- [9] Lipscombe, O. J., Hayden, S. M., Vignolle, B., McMorris, D. F. & Perring, T. G. Persistence of high-frequency spin fluctuations in overdoped superconducting $\text{La}_{2-x}\text{Sr}_x\text{CuO}_4$ ($x = 0.22$). *Phys. Rev. Lett.* **99**, 067002 (2007).
- [10] Dahm, T. et al. Strength of the spin-fluctuation-mediated pairing interaction in a high-temperature superconductor. *Nature Phys.* **5**, 217 (2009).
- [11] Le Tacon, M. et al. Intense paramagnon excitations in a large family of high-temperature superconductors. *Nature Phys.* **7**, 725 (2011).
- [12] Anderson, P. W. The resonating valence bond state in La_2CuO_4 and superconductivity. *Science* **235**, 1196 (1987).
- [13] Ch.-M. Ho, Muthukumar, V. N., Ogata, M. & Anderson, P. W. Nature of spin excitations in two-dimensional Mott insulators: undoped cuprates and other materials. *Phys. Rev. Lett.* **86**, 1626 (2001).
- [14] Christensen, N. B. et al. Quantum dynamics and entanglement of spins on a square lattice. *Proc. Nat. Acad. Sciences* **104**, 15264 (2007).
- [15] Dalla Piazza, B. et al. Fractional excitations in the square-lattice quantum antiferromagnet. *Nature Phys.* **11**, 62 (2015).
- [16] Ebrahimnejad, H., Sawatzky, G. A. & Berciu, M. The dynamics of a doped hole in a cuprate is not controlled by spin fluctuations. *Nature Phys.* **10**, 951 (2014).
- [17] Powalski, M., Uhrig, G. S. & Schmidt, K. P. Roton minimum as a fingerprint of magnon-Higgs scattering in ordered quantum antiferromagnets. *Phys. Rev. Lett.* **115**, 207202 (2015).
- [18] Sandvik, A. W. & Singh, R. R. P. High-energy magnon dispersion and multimagnon continuum in the two-dimensional Heisenberg antiferromagnet. *Phys. Rev. Lett.* **86**, 528 (2001).
- [19] Syromyatnikov, A. V. Spectrum of short-wavelength magnons in a two-dimensional quantum Heisenberg antiferromagnet on a square lattice: third-order expansion in $1/S$. *J. Phys. C* **22**, 216003 (2010).
- [20] Knetter, C. & Uhrig, G. S. Perturbation theory by flow equations: dimerized and frustrated $S = 1/2$ chain. *Eur. Phys. J. B* **13**, 209 (2000).
- [21] See also Methods Section.
- [22] Knetter, C., Schmidt, K. P. & Uhrig, G. S. The structure of operators in effective particle-conserving models. *J. Phys. A: Math. Gen.* **36**, 7889 (2003).
- [23] Rønnow, H. M. et al. Spin dynamics of the 2D spin $\frac{1}{2}$ quantum antiferromagnet copper deuteroformate tetradeuterate (CFTD). *Phys. Rev. Lett.* **87**, 037202 (2001).
- [24] Canali, C. M. & Girvin, S. M. Theory of Raman scattering in layered cuprate materials. *Phys. Rev. B* **45**, 7127 (1992).
- [25] Canali, C. M. & Wallin, M. Spin-spin correlation functions for the square-lattice Heisenberg antiferromagnet at zero temperature. *Phys. Rev. B* **48**, 3264 (1993).
- [26] Weidinger, S. A. & Zwerger, W. Higgs mode and magnon interactions in 2D quantum antiferromagnets from Raman scattering. *Eur. Phys. J. B* **88**, 237 (2015).
- [27] Coldea, R. et al. Spin Waves and Electronic Interactions in La_2CuO_4 . *Phys. Rev. Lett.* **86**, 5377 (2001).

Acknowledgements

We gratefully acknowledge the Helmholtz Virtual Institute “New states of matter and their excitations” for financial support. M.P. was also supported by the Cusanus Werk. Experimental data was kindly provided by N. B. Christensen and H. M. Rønnow.

Competing financial interests

The authors declare that they have no competing financial interests.

Author contributions

M.P. performed the numerical computations. All authors contributed to the theoretical concepts, the interpretation of the results, and the writing of the paper.